DOI: 10.1002/ejic.200600085

# Structural and Magnetic Studies of Copper(II) and Zinc(II) Coordination Complexes Containing Nitroxide Radicals as Chelating Ligands

**Akihiro Ito,[a] Yoshiaki Nakano,[a] Masashi Urabe,[a] Kazuyoshi Tanaka,*[a,b] and Motoo Shiro[c]**

**Keywords:** Copper / Density functional calculations / Magnetic properties / Radicals / Zinc

The mononuclear transition metal complexes $[Cu(CF_3SO_3)_2\mathbf{1}_2]$ (**1a**), $[Zn(CF_3SO_3)_2\mathbf{1}_2]$ (**1b**), $[Cu(CF_3SO_3)_2\mathbf{2}_2]\cdot 2CH_3CN$ (**2a**), and $[Zn(CF_3SO_3)_2\mathbf{2}_2]\cdot 2CH_3CN$ (**2b**) have been prepared from the newly synthesized doxyl nitroxide ligands 4,4-dimethyl-2,2-di(2-pyridyl)oxazolidine-*N*-oxyl (**1**) and 4,4-dimethyl-2,2-bis[2-(3-methylpyridyl)]oxazolidine-*N*-oxyl (**2**) and $M(CF_3SO_3)_2$ (M = $Cu^{II}$ or $Zn^{II}$). These metal–nitroxide complexes have been structurally and magnetically characterized. In all complexes, the four pyridyl groups coordinate in equatorial coordination sites and the two nitroxide groups in axial coordination sites, which means that the central metal ion acquires a distorted $N_4O_2$ octahedral configuration. The variable-temperature magnetic susceptibility data show that complexes **1b** and **2b** exhibit paramagnetic behavior, and hence a very weak intraligand magnetic interaction could be estimated [$J_{NO-NO}$ = –0.64 (**1b**) and 0.14 $cm^{-1}$ (**2b**)]. The $\chi_m T$ values of **1a** and **2a** decrease continuously with decreasing temperature until they reach a nearly constant value at around 50 K, thereby indicating an intramolecular antiferromagnetic interaction between the $Cu^{II}$ ion and the nitroxide ligands for both **1a** and **2a** [$J_{Cu-NO}$ = –81.6 (**1a**) and –78.1 $cm^{-1}$ (**2b**)]. These magnetic behaviors are supported by density functional theory calculations and are discussed in connection with the specific structural features.


## Introduction

Studies in multi-spin systems consisting of paramagnetic metal ions and organic radicals are drawing much attention in the field of molecular magnetism.[1] The advantage of using metal–radical compounds resides not only in the fact that both building blocks afford spin centers but also that a higher dimensional molecular architecture can be constructed by versatile coordination patterns of paramagnetic metal ions. Moreover, the radical ligands have the possibility of mediating a stronger magnetic interaction between the adjacent paramagnetic metal ion centers even though the metal–metal distance is large. Therefore, the metal–radical approach has become one of the most promising strategies for large hetero-spin assemblies of exchange-coupled species.

On the other hand, as is the case with metal–radical complexes in which the radical centers are directly bound to the paramagnetic metal ions, intramolecular magnetic interactions are governed by direct overlap between their magnetic orbitals.[2,3] Hence, the nature of the magnetic interaction depends strongly on the coordination geometry around the paramagnetic metal ion. For example, the magnetic interactions in copper(II)–radical complexes range from strong antiferromagnetic interactions to weak ferromagnetic ones.[2] Therefore, the development of organic radical ligands is important to control the magnetic interaction. Several kinds of organic radical ligands have been studied in this context.[4–7] In particular, nitroxide radicals have often been used as paramagnetic ligand molecules because of their stability and ease of chemical modification.[3] However, nitroxides are generally considered as weak Lewis bases and hence they cannot coordinate to metal ions unless the Lewis acidity of the metal center is enhanced by using electron-withdrawing co-ligands such as hexafluoroacetylacetonato (hfac). Consequently, their weak ligating ability to metal ions prevents the formation of metal–nitroxide complexes with high-dimensional structures.[3] Actually, the dimensionality is restricted due to the prior occupation of coordination sites by the electron-withdrawing co-ligands.[8,9] Two strategies have been developed to overcome this difficulty. One approach is to use a high-spin poly(nitroxide radical) as a polydentate bridging ligand to connect the paramagnetic metal ions.[10,11] The other approach is to incorporate nitroxide groups into normal organic ligands with powerful ligating ability such as pyridine,[12] 2,2′-bipyridine,[13] triazole,[14] imidazole,[15] and piperazine,[16]

[a] Department of Molecular Engineering, Graduate School of Engineering, Kyoto University,
Sakyo-ku, Kyoto 606-8501, Japan
E-mail: a51053@sakura.kudpc.kyoto-u.ac.jp
[b] CREST, Japan Science and Technology Agency (JST), Japan
[c] Rigaku Corporation, X-ray Research Laboratory, Matsubaracho 3-9-12, Akishima, Tokyo 196-8666, Japan

  

which allows a facile coordination to metal ions through the chelate effect.

In the present work, two new organic radical ligands bearing pyridyl groups, namely 4,4-dimethyl-2,2-di(2-pyridyl)oxazolidine-*N*-oxyl (**1**) and 4,4-dimethyl-2,2-bis[2-(3-methylpyridyl)]oxazolidine-*N*-oxyl (**2**), were synthesized to have a suitable ligating ability to metal ions. The selection of copper(II) and zinc(II) as the metal ion centers stems from two reasons: (i) $Cu^{II}$ has a $d^9$ configuration with spin-1/2, which simplifies the magnetic interaction between the metal ion and the organic radical ligand,[3] and (ii) $Zn^{II}$ has a closed-shell $d^{10}$ configuration with no unpaired electrons, and hence we can extract the direct magnetic interaction between the paramagnetic ligand molecules. More conveniently, the ionic radius for $Cu^{II}$ (0.87 Å) is almost the same as that for $Zn^{II}$ (0.88 Å).[17] Structural characterization by X-ray crystallographic studies and measurement of the magnetic properties with a SQUID magnetometer for the newly prepared metal–radical complexes were performed. For the $Cu^{II}$ and $Zn^{II}$ complexes with **1**, a theoretical analysis was also carried out on the basis of density functional calculations.

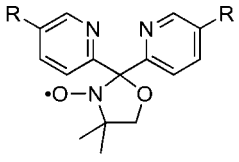

**1**: R = H
**2**: R = $CH_3$

## Results and Discussion

### Synthesis

The novel radical ligands **1** and **2** were synthesized as illustrated in Scheme 1.

Coupling of the dipyridyl ketone **3** (or **4**), with 2-amino-2-methylpropan-1-ol in toluene gives the oxazolidine **5** (or **6**), in high yield. A long reaction time (several days) and continuous water removal by means of a Dean–Stark trap were needed for successful preparation of **5** and **6**. Dipyridyl ketone **4** was prepared by reaction of ethyl chloroformate with lithiated 2-bromo-5-methylpyridine, whereas **3** is commercially available. Oxidation of **5** and **6** with MCPBA in $Et_2O$ finally gave **1** and **2** in relatively high yield. The four complexes **1a**, **1b**, **2a**, and **2b** were obtained by treatment of an acetonitrile solution of $M(CF_3SO_3)_2$ (M = $Cu^{II}$ and $Zn^{II}$) with the corresponding radical ligand, **1** and **2**; vapor diffusion of $Et_2O$ into the reaction mixtures afforded single crystals of these complexes. Elemental analyses of complexes **1a** and **1b** confirmed that the two radical ligands coordinate to a single metal ion. On the other hand, efflorescence was observed with complexes **2a** and **2b**, which suggests that some solvent molecules are included in the crystals. Consequently, we could not determine the chemical formulae of **2a** and **2b** from the elemental analyses; they were finally determined by the X-ray structure analyses, as discussed below.

### Crystal Structures

The structures of complexes **1a**, **1b**, **2a**, and **2b** were determined by X-ray crystallography at 103 or 123 K. All the

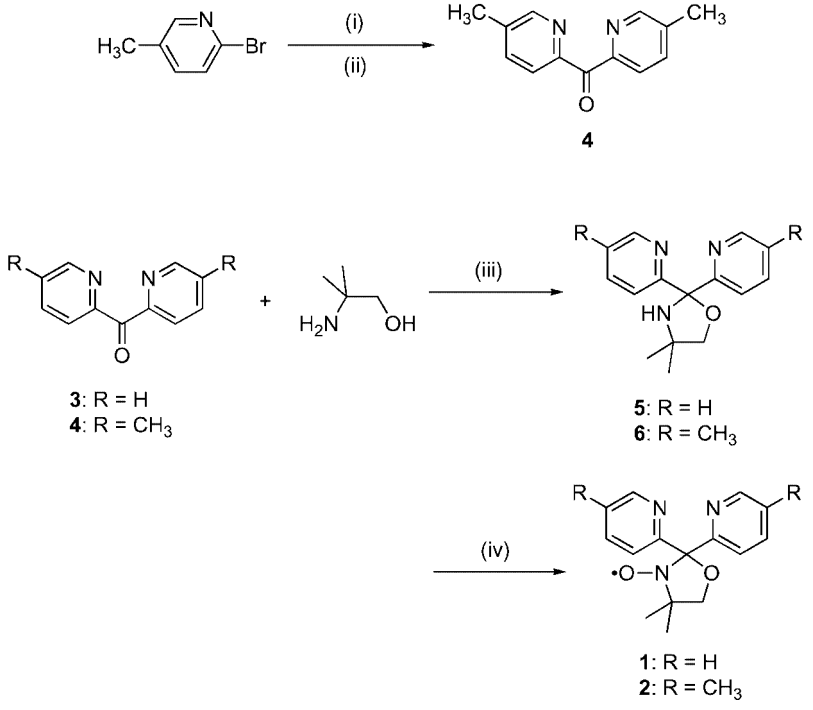

Scheme 1. Synthesis of **1** and **2**: (i) *n*BuLi, THF, –80 °C; (ii) $ClCO_2Et$, THF, –80 °C; (iii) toluene, $H_2SO_4$, reflux (–$H_2O$); (iv) MCPBA, $Et_2O$, 0 °C.

  

Table 1. Selected bond lengths [Å], bond angles [°], and dihedral angles [°] for **1a**, **1b**, **2a**, and **2b**.

| | **1a** | **1b** | **2a** | | **2b** | |
|---|---|---|---|---|---|---|
| M–N2 | 2.001(1) | 2.101(1) | 2.014(2) | 2.025(2) | 2.101(2) | 2.096(2) |
| M–N3 | 2.033(1) | 2.144(1) | 2.028(2) | 2.001(2) | 2.134(2) | 2.119(2) |
| M–O1 | 2.333(1) | 2.163(1) | 2.333(2) | 2.309(2) | 2.165(1) | 2.155(2) |
| N2–M–N3 | 86.52(6) | 85.24(5) | 86.53(8) | 87.66(8) | 85.03(7) | 86.46(6) |
| M–O1–N1 | 110.3 | 114.2 | 110.9 | 109.7 | 114.7 | 113.3 |
| $\varphi$[a] | 90.5 | 91.4 | 94.8 | 83.8 | 85.5 | 96.4 |
| $\theta$[b] | 6.0 | 5.6 | 5.9 | 4.7 | 5.8 | 5.1 |

[a] Dihedral angle between the equatorial plane and the nitroxide plane (see text). [b] Tilt angle of the $Cu^{II}$–$O_{NO}$ coordination bond from the line perpendicular to the equatorial plane of the $Cu^{II}$ ion (see text).

complexes crystallize in the triclinic system with space group $P\bar{1}$; they are isostructural. The nitroxide ligand molecule **1** or **2** in these complexes behaves as a tridentate ligand through two pyridyl N-atoms ($N_{pyridyl}$) and one nitroxide O-atom ($O_{NO}$). All the equatorial coordination sites around the central metal ion are occupied by the $N_{pyridyl}$ atoms, with the remaining axial coordination sites occupied by $O_{NO}$ atoms. As a result, the central metal ion has a distorted $N_4O_2$ octahedral configuration. The triflate anions are not coordinated. Selected bond lengths, bond angles, and dihedral angles are given in Table 1, where the dihedral angle, $\varphi$, is defined as that between the equatorial plane (defined by the central metal ion and the four $N_{pyridyl}$ atoms) and the nitroxide plane (defined by the nitroxide N- and O-atoms and two carbon atoms adjacent to the nitroxide N-atom). The tilt angle, $\theta$, is defined as the difference between the line along the $Cu^{II}$–$O_{NO}$ coordination bond and the line perpendicular to the equatorial plane of the $Cu^{II}$ ion.

### *[Cu(CF$_3$SO$_3$)$_2$1$_2$] (1a) and [Zn(CF$_3$SO$_3$)$_2$1$_2$] (1b)*

The molecular structures of **1a** and **1b** are shown in Figure 1. The central $Cu^{II}$ and $Zn^{II}$ ions reside at the inversion center of a distorted octahedron. In the equatorial plane, a considerable deviation from the ideal square geometry is seen in **1a**: the two kinds of $Cu^{II}$–$N_{pyridyl}$ bond lengths are Cu–N2 = 2.001(1) and Cu–N3 = 2.033(1) Å, and the N2–Cu–N3 angle is 86.52(6)°. The axially coordinated $Cu^{II}$–$O_{NO}$ bond [Cu–O1 = 2.333(1) Å] is longer than the equatorially coordinated $Cu^{II}$–$N_{pyridyl}$ bonds. As is well-known for a $d^9$ electron configuration like the $Cu^{II}$ ion, the octahedral geometry does not remain perfect at equilibrium and is inevitably distorted along one axis (the Jahn–Teller effect).[18]

A similar deviation from the ideal square geometry is also observed in **1b** [Zn–N2 = 2.101(1), Zn–N3 = 2.144(1) Å; N2–Zn–N3 = 85.24(5)°]. The elongation along the axial axis is not conspicuous due to the $d^{10}$ electron configuration of the $Zn^{II}$ ion [Zn–O1 = 2.163(1) Å]. The dihedral ($\varphi$) and tilt ($\theta$) angles in **1a** (and **1b**) are 90.5° (91.4°) and 6.0° (5.6°), respectively. As the elongation axis is through O1–Cu1–O1*, the magnetic orbital of $Cu^{II}$ is considered to be $d_{x^2-y^2}$, which is directed toward the nitrogen atoms of the pyridyl groups. As shown in part a of Figure 2, neighboring complex molecules in **1a** (and also **1b**) are well separated in the crystal [the shortest distances between the adjacent metal ions for **1a** and **1b** are 7.5928(5) and 7.6792(4) Å, respectively]. The shortest $O_{NO}$–$O_{NO}$ distances between intermolecular nitroxide groups for **1a** and **1b** are 5.680(2) and 5.953(2) Å, respectively. There is a short C–C contact [3.337(3) Å for **1a** and 3.323(3) Å for **1b**] that is less than the sum of the van der Waals radii (3.40 Å)[19] between the adjacent complex molecules along the *a*-axis.

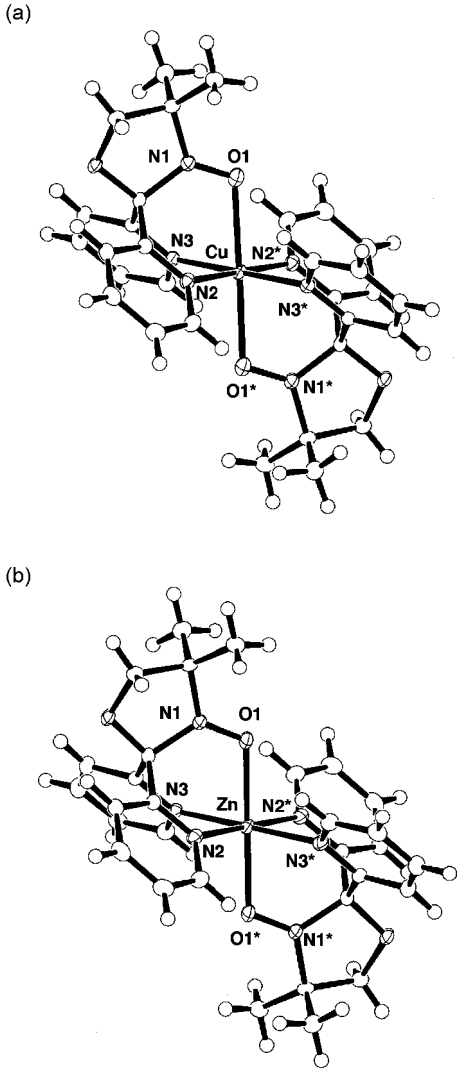


Figure 1. ORTEP view (50% probability ellipsoids) and atom labeling scheme of a) [Cu(CF$_3$SO$_3$)$_2$**1**$_2$] (**1a**) and b) [Zn(CF$_3$SO$_3$)$_2$**1**$_2$] (**1b**). The non-coordinated triflate anions have been omitted for clarity. The atom labeling for compounds **2a** and **2b** is identical.

  

As described later, however, the spin density on the C atoms with the short contact is so small that a strong magnetic interaction via this molecular contact cannot be expected. Consequently, the magnetic systems of **1a** and **1b** can be considered to be an assemblage of well-isolated three- and two-spin systems, respectively. Moreover, **1a** and **1b** have similar molecular and crystal structures, and therefore we can compare the magnetic interactions in the three-spin systems with those in the two-spin system without the central spin-1/2 moiety within the same geometrical configuration.

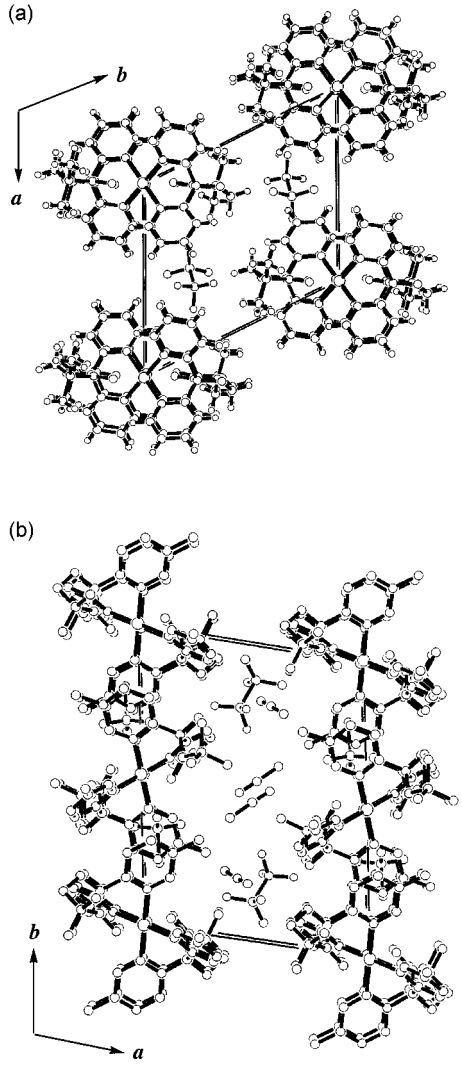


Figure 2. Views of the crystal packing for **1a** (a) and **2a** (b).

### *[Cu(CF$_3$SO$_3$)$_2$2$_2$]·2CH$_3$CN (2a) and [Zn(CF$_3$SO$_3$)$_2$2$_2$]·2CH$_3$CN (2b)*

The crystal structure of **2a** is shown in Figure 2 (b). The crystal of **2a** (and also **2b**) contains two acetonitrile molecules per molecular unit and is different from **1a** (and **1b**) as there are two crystallographically independent molecules in which the central metal ion resides on the inversion center. The molecular structures of **2a** and **2b** are similar to those of **1a** and **1b**. The characteristic geometrical parameters of **2a** are as follows: Cu–O1 = 2.333(2) [2.309(2)], Cu–N2 = 2.014(2) [2.025(2)], Cu–N3 = 2.028(2) Å [2.001(2) Å]; the N2–Cu–N3 angle is 86.53(8)° [87.66(8)°]. The corresponding parameters in **2b** are also similar to those of **1b**: Zn–O1 = 2.165(1) [2.155(2)], Zn–N2 = 2.101(2) [2.096(2)], Zn–N3 = 2.134(2) Å [2.119(2) Å], N2–Zn–N3 = 85.03(7)° [86.46(6)°]. Moreover, the dihedral ($\varphi$) and tilt ($\theta$) angles in **2a** (and **2b**) are 94.8° [83.8°] (85.5° [96.4°]) and 5.9° [4.7°] (5.8° [5.1°]), respectively. The deviation of the dihedral angle between the equatorial plane and the nitroxide plane from 90° in **2a** and **2b** is larger than that in **1a** and **1b**. The intermolecular distances in **2a** and **2b** are larger than those in **1a** and **1b** due to the steric hindrance of the crystallized acetonitrile molecules and the methyl group of ligand **2** (the shortest distances between the adjacent metal ions for **2a** and **2b** are 7.97 and 8.16 Å, respectively). The shortest $O_{NO}$–$O_{NO}$ distances between intermolecular nitroxide groups for **2a** and **2b** are 7.477(3) and 7.465(3) Å, respectively. In addition, there is no intermolecular contact less than the sum of the van der Waals radii (3.40 Å for C–C; 3.22 Å for C–O)[19] between the adjacent complex molecules. Therefore, the intermolecular magnetic interactions in **2a** and **2b** are expected to be weaker than those in **1a** and **1b**.

### Magnetic Properties

The temperature-dependent magnetic susceptibility of complexes **1a**, **1b**, **2a**, and **2b** was measured in the temperature range 2–300 K; $\chi_m T$ values are plotted as a function of

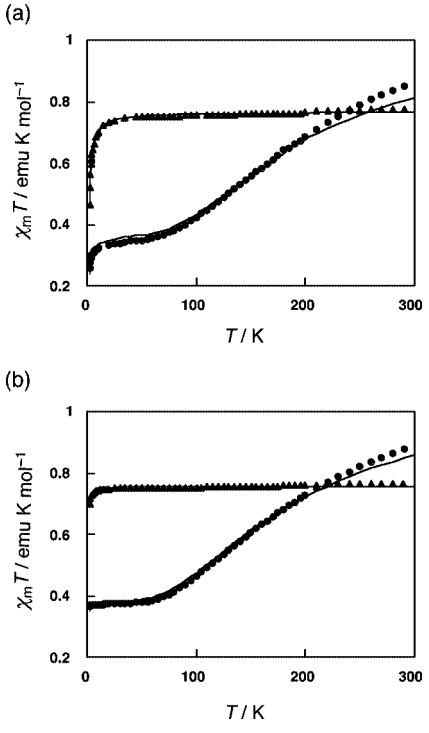


Figure 3. Temperature-dependence of the magnetic susceptibilities of a) **1a** (solid circle) and **1b** (solid triangle) and b) **2a** (solid circle) and **2b** (solid triangle). The solid curves represent the best theoretical fit to the data (see text).

  

the temperature in Figure 3, where $\chi_m$ is the molar magnetic susceptibility per molecular unit.

### *[Cu(CF$_3$SO$_3$)$_2$I$_2$] (1a) and [Zn(CF$_3$SO$_3$)$_2$I$_2$] (1b)*

As shown in Figure 3 (a), the $\chi_m T$ value for **1b** is nearly constant at around 0.75 emu K mol$^{-1}$, which corresponds to two magnetically uncoupled spins-1/2 per molecular unit. This result is reasonable for the complex of a diamagnetic $Zn^{II}$ ion with two spin-1/2 radical ligands. Moreover, the crystal structural analysis shows that the shortest $O_{NO}$–$O_{NO}$ distance between intermolecular nitroxide groups (5.95 Å) is longer than that between intramolecular nitroxide groups (4.33 Å). This indicates that the spin system in **1b** can be regarded as an assemblage of approximately isolated two-spin clusters. Taking these results into account, the magnetic data for **1b** were analyzed by using the Bleaney–Bowers equation[20] for a two-spin cluster composed of a pair of nitroxide radical ligands ($H = -2J_{NO-NO}\boldsymbol{S}_{NO}\cdot\boldsymbol{S}_{NO}$, where $\boldsymbol{S}_{NO}$ is the spin-1/2 operator for the nitroxide radical ligand and $J_{NO-NO}$ is the exchange coupling constant between two intramolecular nitroxide spins). Furthermore, the Curie–Weiss law can be used to describe inter-cluster magnetic interactions [Equation (1)], where $f$ is the purity factor of the sample, $N_A$ the Avogadro number, $g$ the isotropic $g$-factor (assuming $g = 2$), $\theta$ the Weiss temperature, $k_B$ the Boltzmann constant, and $\mu_B$ the Bohr magneton.

$$\chi_m T = f\frac{2N_A g^2 \mu_B^2 T}{k_B(T-\theta)}\frac{1}{3+exp\left(-\frac{2J_{NO-NO}}{k_B T}\right)} \quad (1)$$

The best fit parameters were found to be $f = 1.02$, $J_{NO-NO} = -0.64$ cm$^{-1}$, and $\theta = -0.4$ K ($-0.26$ cm$^{-1}$). The small values of $J_{NO-NO}$ and $\theta$ indicate that the intra- and intermolecular magnetic interaction between the nitroxide radical spins in **1b** can be ignored as compared to the magnetic interaction between the d$^9$ $Cu^{II}$ spin and the nitroxide radical spin in the complex molecule of **1a**, as discussed below.

In contrast, the $\chi_m T$ value for **1a** at room temperature is smaller than the theoretical value ($\chi_m T$ = 1.125 emu K mol$^{-1}$) for three spins-1/2 per molecular unit. Furthermore, on lowering the temperature, the $\chi_m T$ value decreases gradually and reaches a nearly constant value close to a theoretical value for a single spin-1/2 per molecular unit ($\chi_m T$ = 0.375 emu K mol$^{-1}$) at around 50 K. These results indicate that a relatively strong antiferromagnetic interaction is present in the crystal of **1a**. As indicated by the crystal structure analysis of **1a**, the shortest intra- and intermolecular $O_{NO}$–$O_{NO}$ distances between the nitroxide radical ligands (4.67 and 5.68 Å, respectively) and the shortest intermolecular $Cu^{II}$–$Cu^{II}$ distance (7.59 Å) are longer than the $Cu^{II}$–$O_{NO}$ distance (2.333 Å). This indicates that the spin system in **1a** can be regarded as an assemblage of approximately isolated three-spin clusters consisting of a $Cu^{II}$ ion and two nitroxide radical ligands. Moreover, the direct intramolecular magnetic interaction between the nitroxide ligand molecules in **1a** can be neglected due to the magnetic behavior of **1b**. Therefore, the arrangement of the three-spin clusters in complex **1a** can be regarded as a linear three-spin model [$\boldsymbol{S}_{NO(1)}$–$\boldsymbol{S}_{Cu}$–$\boldsymbol{S}_{NO(2)}$]. The spin Hamiltonian can be written as shown in Equation (2) using an exchange coupling constant, $J_{Cu-NO}$, between the $Cu^{II}$ spin and the nitroxide radical spin.

$$H = -2J_{Cu-NO}[\boldsymbol{S}_{NO(1)}\cdot\boldsymbol{S}_{Cu} + \boldsymbol{S}_{Cu}\cdot\boldsymbol{S}_{NO(2)}] \quad (2)$$

for which the eigenvalues are

$$E_1(S = 1/2) = 2\,J_{Cu-NO}$$

$$E_2(S = 1/2) = 0$$

$$E_3(S = 3/2) = -\,J_{Cu-NO}$$

Hence, the temperature dependence of $\chi_m T$ is given by Equation (3).

$$\chi_m T = f\frac{N_A g^2 \mu_B^2 T}{4k_B(T-\theta)}\frac{1+exp\left(-\frac{2J_{Cu-NO}}{k_B T}\right)+10exp\left(\frac{J_{Cu-NO}}{k_B T}\right)}{1+exp\left(-\frac{2J_{Cu-NO}}{k_B T}\right)+2exp\left(\frac{J_{Cu-NO}}{k_B T}\right)} \quad (3)$$

The parameters in this equation are the same as in Equation (1). This equation was fitted well to the experimental data, and the best-fit parameters were $f = 0.99$, $J_{Cu-NO} = -81.6$ cm$^{-1}$, and $\theta = -1.1$ K ($-0.77$ cm$^{-1}$). The sign of $J_{Cu-NO}$ is opposite to that found for $Cu^{II}$–nitroxide complexes where the $O_{NO}$ atoms occupy the axial positions (+10 to +70 cm$^{-1}$).[2,21] However, the magnitude of $J_{Cu-NO}$ is smaller than that observed for $Cu^{II}$–nitroxide complexes where the $O_{NO}$ atoms occupy the equatorial positions (ca. $-600$ cm$^{-1}$).[2,21] This discrepancy in the sign of $J_{Cu-NO}$ suggests that the overlap mode between the π* orbital of the nitroxide group and the magnetic orbital ($d_{x^2-y^2}$) of the $Cu^{II}$ ion differs between the present complex and the previously reported axially coordinated $Cu^{II}$–nitroxide complexes.[22] The relatively small $J_{Cu-NO}$ value arises from the fact that the Cu–$O_{NO}$ distance is fairly long (ca. 2.3 Å) owing to the Jahn–Teller distortion as compared to that for the equatorially coordinated $Cu^{II}$–nitroxide complexes (ca. 2.0 Å).[21,23,24]

### *[Cu(CF$_3$SO$_3$)$_2$2$_2$]·2CH$_3$CN (2a) and [Zn(CF$_3$SO$_3$)$_2$2$_2$]·2CH$_3$CN (2b)*

The $\chi_m T$ vs. $T$ plots for **2a** and **2b** are shown in Figure 3 (b). The temperature dependence of the $\chi_m T$ value for **2a** and **2b** is similar to those for **1a** and **1b**, respectively. The X-ray structural analysis shows that the intermolecular distance and shortest contacts in **2a** and **2b** are larger than those in **1a** and **1b**. However, the temperature dependence of their magnetic properties remains unchanged. This means that the main magnetic interaction observed in the crystals of **1a** and **2a** can be ascribed to the intramolecular antiferromagnetic interaction between the $Cu^{II}$ spin and the nitroxide radical spin. Hence, the magnetic data were again fitted to Equations (1) and (3). The best fit, shown in Figure 3 (b) as a solid line, afforded the following parameters:

  

$f$ = 1.03, $J_{Cu-NO}$ = –78.1 cm$^{-1}$, and $\theta$ = –0.2 K (–0.15 cm$^{-1}$) for **2a** and $f$ = 1.01, $J_{NO-NO}$ = 0.14 cm$^{-1}$, and $\theta$ = –0.3 K (–0.19 cm$^{-1}$) for **2b**. The value of $J_{Cu-NO}$ is similar to that for **1a**, which supports the assumption that the spin alignment in **1a** and **2a** is governed by an intramolecular antiferromagnetic interaction between the Cu$^{II}$ ion and the nitroxide ligands.

### Theoretical Considerations

On the basis of the obtained X-ray structures of **1a** and **1b** we performed quantum chemical calculations in order to examine the electronic structures of the present metal–radical complexes. First of all, we investigated the spin-density distribution of complexes **1a** and **1b**. As density functional theory (DFT) calculations often give good results for both signs and magnitudes of spin densities of open-shell molecules, we carried out calculations using the hybrid HF/DF method (B3LYP/LANL2DZ).[25] The partially occupied spin-free natural orbitals from the B3LYP/LANL2DZ calculations for the $^4A_u$ state of **1a** and the selected spin densities of the low- and high-spin states of **1a** and **1b** are shown in Figures 4 and 5, respectively. In both of the doublet and quadruplet states of **1a**, the spin densities are mainly localized on the Cu$^{II}$ ion and the nitroxide groups. In **1b**, the spin densities for the singlet and triplet states are localized only on the nitroxide groups of the two ligands. On the other hand, the spin densities over the peripheral pyridyl groups of **1a** and **1b** are quite small. These results are consistent with the experimental result that the intermolecular magnetic interactions in all four complexes are very weak.

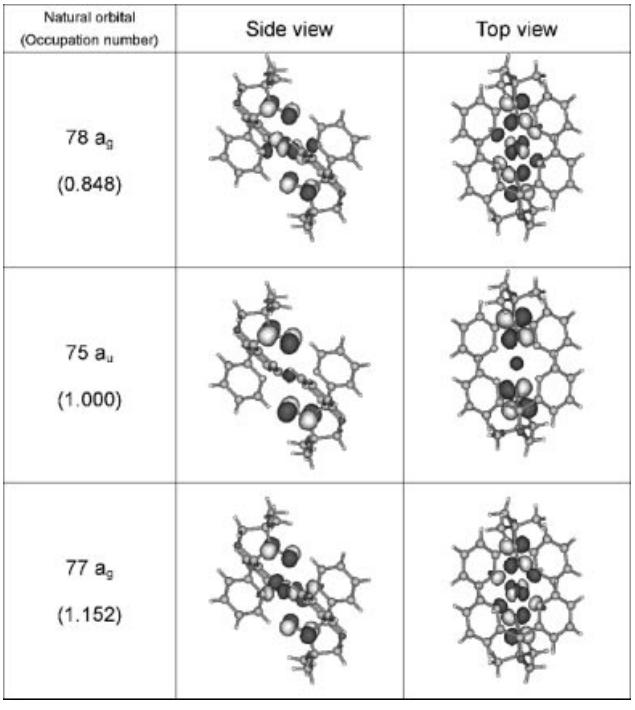


Figure 4. Three partially occupied natural orbitals for the $^2A_u$ state of **1a** at the UB3LYP/LANL2DZ level of theory.

Moreover, the sign of the spin density on the Cu$^{II}$ ion in the doublet state of **1a** is opposite to that in the quadruplet state, while the magnitudes of the spin densities on the Cu$^{II}$ and nitroxyl groups remain unchanged. This indicates that an antiferromagnetic spin alignment occurs in the doublet state of **1a**, while a ferromagnetic spin alignment occurs in the quadruplet state of **1a**. In addition, the natural orbital occupation number indicates that the $^2A_u$ state of **1a** has a doublet triradical character.

Energetically, the doublet state ($^2A_u$) in **1a** was estimated to be more stable than the quadruplet state ($^4A_u$) by 223 cm$^{-1}$. In addition, the exchange coupling constant, $J$, can be estimated to be 110 cm$^{-1}$ by using the approximate spin projection method[26–29] given by Equation (4),

$$J = \frac{E(^2A_u) - E(^4A_u)}{\langle S^2\rangle(^4A_u) - \langle S^2\rangle(^2A_u)} \quad (4)$$

where $E(^2A_u)$ and $E(^4A_u)$ are the total energies for the $^2A_u$ and $^4A_u$ states and $<S^2>(^2A_u)$ and $<S^2>(^4A_u)$ the expectation values for the total spin angular momentums of $^2A_u$ and $^4A_u$ states. The estimated $J$ value gives a good agreement with the $J_{Cu-NO}$ value determined from the magnetic

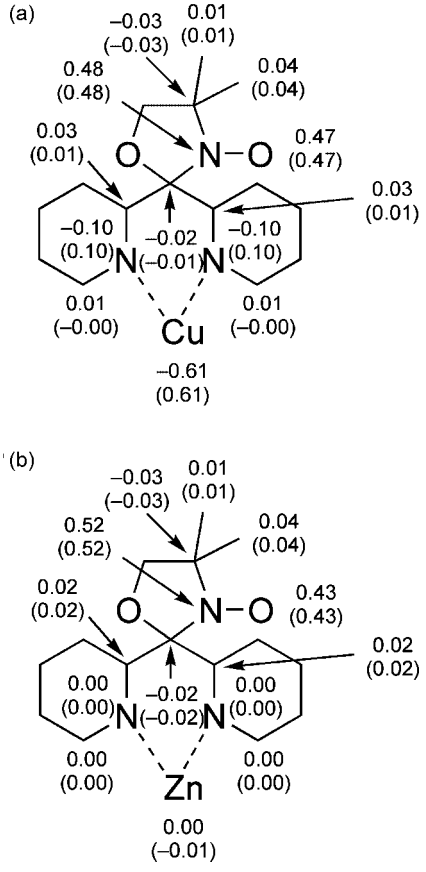


Figure 5. Mulliken spin density for a) the doublet and quadruplet states (in parentheses) of **1a** and b) the singlet and triplet states (in parentheses) of **1b** at the UB3LYP/LANL2DZ level of theory. The centrosymmetric atoms have the same spin density (having the opposite sign only for the singlet state of **1b**), hence one of the two ligands has been omitted for clarity.

  

measurements. On the other hand, the singlet ($^1A_u$) and triplet ($^3A_u$) states of **1b** were found to be virtually degenerate. This indicates that effective magnetic interactions between the two nitroxide ligands via the diamagnetic $Zn^{II}$ ion do not occur.

The present axially coordinated $Cu^{II}$–nitroxide complexes **1a** and **2a** show antiferromagnetic coupling between the metal center and the nitroxide ligand molecule, although the $Cu^{II}$–nitroxide magnetic interaction in the axially coordinated $Cu^{II}$–nitroxide complexes is usually ferromagnetic.[3,22] Schweizer and co-workers have clearly shown the spin-density distribution of an axially coordinated $Cu^{II}$–nitroxide complex on the basis of a neutron diffraction analysis; their results strongly suggest that the ferromagnetic interaction between the $Cu^{II}$ ion and the nitroxide ligand is derived from orthogonality between the corresponding magnetic orbitals (the $3d_{x^2-y^2}$ atomic orbital for $Cu^{II}$ and the π* orbital for the nitroxide).[30] In general, the exchange parameter is approximately expressed as Equation (5),

$$J_{dir} \approx \rho_{x^2-y^2} J(3d_{x^2-y^2}, \pi^*) \quad (5)$$

$$J(3d_{x^2-y^2}, \pi^*) \sim < 3d_{x^2-y^2}\,\pi^* \mid \pi^*\,3d_{x^2-y^2} > + 2S < \pi^* \mid h \mid 3d_{x^2-y^2} > - S^2 [\, \varepsilon_{xy} + \varepsilon_{\pi^*} + < 3d_{x^2-y^2}\,3d_{x^2-y^2} \mid \pi^*\,\pi^* > ]$$

where $\rho_{x^2-y^2}$ is the density of the unpaired electron on the $3d_{x^2-y^2}$ atomic orbital, $S = <3d_{x^2-y^2}|\pi^*>$ is the overlap integral between the magnetic orbitals, $\varepsilon_{xy}$ and $\varepsilon_{\pi^*}$ are the orbital energies, $<3d_{x^2-y^2}\pi^*|\pi^*\,3d_{x^2-y^2}>$ and $<3d_{x^2-y^2}\,3d_{x^2-y^2}|\pi^*\,\pi^*>$ are the two-electron integrals of the exchange and Coulomb types, respectively, and $h$ is the one-electron Hamiltonian. According to Musin and co-workers,[31] the strong antiferromagnetic coupling ($J \approx -500\ cm^{-1}$)[3] in equatorially coordinated $Cu^{II}$–nitroxide complexes can be explained by the above-mentioned direct exchange interaction $J_{dir}$. The third term of $J(3d_{x^2-y^2}, \pi^*)$ in Equation (5) becomes dominant due to the large overlap integral $S \approx 10^{-1}$ ($J_{dir} \approx -500\ cm^{-1}$).

On the other hand, in axially coordinated $Cu^{II}$–nitroxide complexes, slight delocalization of the unpaired electron from the π* orbital of the nitroxide group to the $3d_{z^2}$ atomic orbital of the $Cu^{II}$ ion takes place. Hence, the delocalized π* orbital is approximately expressed as $\pi^* + c_{z^2}3d_{z^2}$. As a result, the exchange parameter contains two main contributions, $J \approx J_{dir} + J_{del}$. The exchange parameter due to the delocalization mechanism $J_{del}$ takes the form shown in Equation (6),

$$J_{dir} \approx \rho_{x^2-y^2}\rho_{z^2} <3d_{x^2-y^2}\,3d_{z^2}|3d_{z^2}\,3d_{x^2-y^2}> \quad (6)$$

where $\rho_{z^2} = c_{z^2}$, the spin density due to delocalization from the nitroxide group to $Cu^{II}$. In the axially coordinated $Cu^{II}$–nitroxide complexes, the values of $S$ are estimated to be very small because of orthogonality between the $3d_{x^2-y^2}$ atomic orbital for the $Cu^{II}$ ion and the π* orbital of nitroxide group. Hence, the direct exchange term $J_{dir}$ only gives a very small positive value. On the other hand, in spite of the smallness of the delocalization $\rho_{z^2}$, the large intra-atomic exchange integral [Equation (6)] leads to a major contribution from the delocalized exchange term $J_{del}$ (ca. 10–65 $cm^{-1}$).[31]

In the present complexes **1a** and **1b** the nitroxide groups are axially coordinated to the $Cu^{II}$ ion. However, the determined exchange parameter is antiferromagnetic ($J_{exp} \approx 80\ cm^{-1}$), which is contrary to the expected ferromagnetic interaction in axially coordinated $Cu^{II}$–nitroxide complexes. This can be explained by the difference of overlap mode between the magnetic orbitals of the $Cu^{II}$ ion and the nitroxide groups. As shown in Figure 6 (a), when the symmetry plane containing the π* orbital of the nitroxide group is orthogonal to the equatorial plane of the $Cu^{II}$ ion, the tilting of the $Cu^{II}$–$O_{NO}$ coordination bond from the line

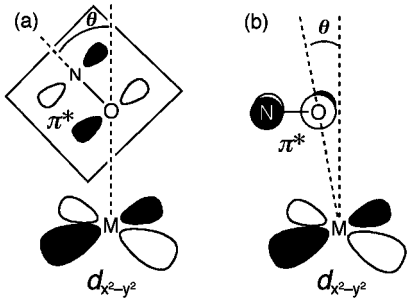


Figure 6. Schematic views of possible orbital interactions between the magnetic orbitals ($3d_{x^2-y^2}$) of the $Cu^{II}$ ion ($3d_{x^2-y^2}$) and the nitroxide radical (π*). $\theta$ is the tilt angle of the $Cu^{II}$–$O_{NO}$ coordination bond from the line perpendicular to the equatorial plane of the $Cu^{II}$ ion.

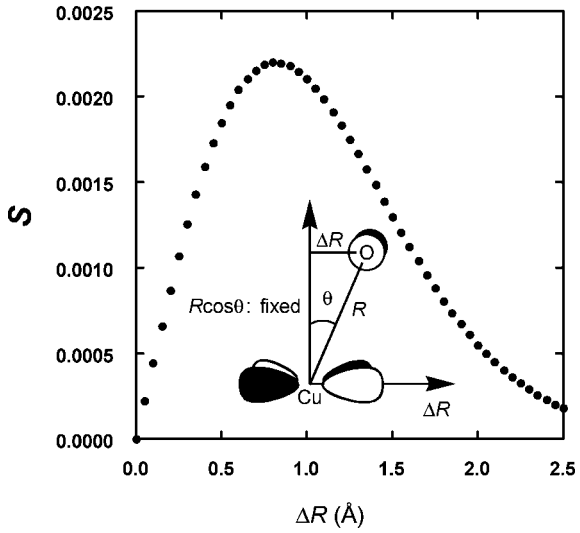


Figure 7. Dependence of the overlap integral between the Slater 2p atomic orbital of the oxygen atom and the Slater $3d_{x^2-y^2}$ atomic orbital of the Cu atom on the distance $\Delta R$ (in Å) defined in the inset ($R\cos\theta$ was fixed to 2.3202 Å, which corresponds to complex **1a**). $\Delta R$ can be related to the tilt angle $\theta$ in Table 1 and Figure 6 by the formula $\sin\theta = \Delta R/R$. We adopted 2.275 and 2.95 for the values of $\zeta$ of the oxygen 2p orbital and the copper 3d orbital, respectively [see: J. A. Pople, D. L. Beveridge, *Approximate Molecular Orbital Theory*, McGraw-Hill, New York, **1970**.]. In the case of complex **1a**, the corresponding overlap integral was estimated to be 0.001 [$\Delta R = 0.2438$].

  

perpendicular to the equatorial plane causes an effective overlap between the π* orbital of the nitroxide group and the $3d_{z^2}$ atomic orbital of the $Cu^{II}$ ion. Therefore, the delocalization mechanism [Equation (6)] leads to a relatively large ferromagnetic interaction. On the other hand, as shown in Figure 6 (b), in the present $Cu^{II}$–nitroxide complexes the symmetry plane containing the π* orbital of the nitroxide group is nearly parallel to the equatorial plane of the $Cu^{II}$ ion. Hence, the overlap integral between the π* orbital of the nitroxide group and the $3d_{z^2}$ atomic orbital of the $Cu^{II}$ ion is virtually negligible. Thus, we can ignore the above-mentioned delocalization mechanism in complexes **1a** and **1b**. More importantly, the $Cu^{II}$–$O_{NO}$ coordination bond tilts from the line perpendicular to the equatorial plane ($\theta \approx 5°$) in the present coordination mode [Figure 6 (b)]. Therefore, the finite overlap integral between the π* orbital of the nitroxide group and $3d_{x^2-y^2}$ atomic orbital of the $Cu^{II}$ ion is expected. However, the overlap integral is expected to be small compared to the equatorially coordinated $Cu^{II}$–nitroxide complexes, as shown in Figure 7 ($S \approx 0.001$). Such a specific overlap mode leads to a relatively weak antiferromagnetic interaction ($J \approx 80\ cm^{-1}$) in complexes **1a** and **1b** due to the direct exchange mechanism.

## Concluding Remarks

The synthesis, magnetic properties, and theoretical analysis of $Cu^{II}$ complexes **1a** and **2a** and $Zn^{II}$ complexes **1b** and **2b** containing radical ligands **1** and **2** have been described. It has been shown that the combination of the metal ion and these radical ligands results in formation of isostructural mononuclear complexes. The magnetic properties of the $Zn^{II}$ complex indicate that there is a weak intramolecular magnetic interaction between two nitroxide ligands. On the other hand, the exchange coupling constant $J_{Cu–NO}$ between the $Cu^{II}$ and the nitroxide ligands for **1a** and **2a** was determined to be –81.6 and –78.1 $cm^{-1}$, respectively, thereby indicating an antiferromagnetic interaction. The DFT calculations show that the ground $^2A_u$ state of **1a** has a doublet triradical character and give a reasonable exchange coupling constant $J_{Cu–NO}$ (–110 $cm^{-1}$). Although the present axially coordinated $Cu^{II}$–nitroxide complexes show an antiferromagnetic interaction, this interaction can be attributed to the specific structural features of the coordination pattern of the nitroxide ligand molecules. Unfortunately, the present nitroxide ligand molecules **1** and **2** are contained in mononuclear transition metal complexes. However, it may be possible to build highly dimensional magnetic materials by using radical ligands containing 3- or 4-pyridyl groups to avoid coordination of all the pyridyl groups to a single metal ion.

## Experimental Section

**General Procedures and Materials:** $^1H$ and $^{13}C$ NMR spectra were recorded with a JEOL AL-300 spectrometer, and chemical shifts are given in ppm relative to internal tetramethylsilane (TMS; $\delta$ = 0.0 ppm) for $^1H$ and to $CDCl_3$ for $^{13}C$ NMR spectroscopy. Elemental analyses were performed by the Center for Organic Elemental Microanalysis of Kyoto University. Toluene was distilled from over calcium hydride. 2-Amino-2-methylpropan-1-ol was distilled from over calcium hydride under reduced pressure. THF was distilled from over potassium/benzophenone under argon. *m*-Chloroperbenzoic acid (MCPBA) was obtained commercially (70–75% purity) and used without further purification. All the other purchased reagents and solvents were used without further purification.

**4,4-Dimethyl-2,2-di(2-pyridyl)oxazolidine (5):** This compound was prepared by a modified literature procedure.[32,33] A mixture of bis(2-pyridyl) ketone (9.71 g, 51.7 mmol), freshly distilled 2-amino-2-methylpropan-1-ol (110 mL, 1130 mmol), and concentrated $H_2SO_4$ (25 drops) in toluene (200 mL) was refluxed for 4 d. The water generated was removed by means of a Dean–Stark trap containing 4-Å molecular sieves. The reaction mixture was then cooled to room temperature and concentrated under reduced pressure. Water (200 mL) and $Et_2O$ (100 mL) were added to the resulting residue and then the organic layer was separated. The aqueous layer was extracted with $CH_2Cl_2$ (2 × 100 mL). The combined organic layers were dried with $MgSO_4$ and the solvents evaporated in vacuo. The residue was recrystallized from cyclohexane to afford **5** (4.39 g, 33%) as a white solid. The mother liquor was evaporated and chromatographed on aluminum oxide (ethyl acetate/*n*-hexane = 1:1 as eluent) to afford additional **5** (8.54 g, 65%). The total yield was 98%. $^1H$ NMR (300 MHz, $CDCl_3$): $\delta$ = 8.55 (d, $J$ = 4.0 Hz, 2 H), 7.75 (d, $J$ = 7.9 Hz, 2 H), 7.63 (td, $J$ = 7.7, 1.6 Hz, 2 H), 7.11–7.16 (m, 2 H), 4.26 (br., 1 H), 3.68 (s, 2 H), 1.21 (s, 6 H) ppm. $^{13}C$ NMR (75.5 MHz, $CDCl_3$): $\delta$ = 162.3, 148.5, 136.3, 122.3, 121.2, 98.9, 77.9, 59.6, 26.6 ppm. $C_{15}H_{17}N_3O$: calcd. C 70.56, H 6.71, N 16.46, O 6.27; found C70.28, H 6.71, N 16.55, O 6.30.

**4,4-Dimethyl-2,2-di(2-pyridyl)oxazolidine-*N*-oxyl (1):** This compound was also prepared by a modified literature procedure.[32] Thus, a solution of MCPBA (4.34 g, ca. 17.6 mmol) in $Et_2O$ (40 mL) was added dropwise to an ice-cooled solution of **5** (3.01 g, 11.8 mmol) in $Et_2O$ (40 mL). The resulting solution was allowed to stand for 4 h. Cold 5% $Na_2CO_3$ aqueous solution (40 mL) was then added to the reaction mixture and the aqueous layer was separated. The organic layer was extracted with cold 5% $Na_2CO_3$ aqueous solution (4 × 40 mL) and the aqueous phases were combined. The aqueous phase was extracted with $CH_2Cl_2$ (5 × 40 mL). The combined organic phase was washed with cold 5% $Na_2CO_3$ solution (2 × 40 mL), dried with $MgSO_4$, and the solvents evaporated in vacuo. The resulting orange solid was chromatographed on silica gel (acetone as eluent). A fraction ($R_f$ = 0.61) afforded **1** as an orange solid (1.99 g, 62%). ESR (X-band, toluene): $g$ = 2.0094 and $a_N$ = 13.7 G. $C_{15}H_{16}N_3O_2$: calcd. C 66.65, H 5.97, N 15.55, O 11.84; found C66.74, H 5.92, N 15.48, O 11.84.

**Bis[2-(3-methylpyridyl)] Ketone (4):** Compound **4** was prepared by a modified literature procedure.[34] *n*BuLi (10.5 mmol, 1.5 M in hexane) was added dropwise to a solution of 2-bromo-5-methylpyridine (1.93 g, 11.0 mmol) in THF (15 mL) at –90 °C (petroleum ether/liquid nitrogen) under argon. The resulting solution was stirred at –90 °C for 1 h, and then a solution of ethyl chloroformate (0.58 g, 5.18 mmol) in THF (2 mL) was added rapidly. After stirring overnight, the reaction mixture was concentrated and $CH_2Cl_2$ (100 mL) and water (100 mL) were added. The organic layer was separated and the aqueous layer was extracted with $CH_2Cl_2$ (4 × 50 mL). The combined organic layer was washed with 10% aqueous $NaHCO_3$, dried with $MgSO_4$, and the solvents evaporated in vacuo. The crude product was chromatographed on silica gel (ethyl acetate as eluent). A fraction ($R_f$ = 0.38) afforded **4** as a pale-

  

yellow solid (yield 0.40 g, 36%). $^1$H NMR (300 MHz, $CDCl_3$): $\delta$ = 8.57 (dd, $J$ = 1.5, 0.7 Hz, 2 H), 8.01 (d, $J$ = 7.9 Hz, 2 H), 7.67 (ddd, $J$ = 7.9, 2.2, 0.7 Hz, 2 H), 2.43 (s, 6 H) ppm. $^{13}$C NMR (75.5 MHz, CDCl3): $\delta$ = 192.8, 152.1, 149.7, 137.0, 136.7, 125.0, 18.7 ppm. $C_{13}H_{12}N_2O$: calcd. C 73.56, H 5.70, N 13.20, O 7.54; found C73.28, H 5.85, N 13.06, O 7.48.

**4,4-Dimethyl-2,2-bis[2-(3-methylpyridyl)]oxazolidine (6):** Compound **6** was obtained from **4** by the same procedure as **5**. The reaction mixture was chromatographed on aluminum oxide (ethyl acetate as eluent) to afford **6** as a pale-yellow solid ($R_f$ = 0.83, yield 97%). $^1$H NMR (300 MHz, $CDCl_3$): $\delta$ = 8.37 (s, 2 H), 7.60 (d, $J$ = 7.9 Hz, 2 H), 7.43 (d, $J$ = 8.1 Hz, 2 H), 4.21 (br., 1 H), 3.67 (s, 2 H), 2.27 (s, 6 H), 1.20 (s, 6 H) ppm. $^{13}$C NMR (75.5 MHz, $CDCl_3$): $\delta$ = 159.7, 148.9, 136.9, 131.6, 120.7, 98.9, 77.9, 59.7, 26.7, 18.0 ppm. $C_{17}H_{21}N_3O$: calcd. C 72.06, H 7.47, N 14.83, O 5.65; found C 72.15, H 7.68, N 14.58, O 5.52.

**4,4-Dimethyl-2,2-bis[2-(3-methylpyridyl)]oxazolidine-*N*-oxyl (2):** Compound **2** was obtained from **6** by the same procedure as **1**. The reaction mixture was chromatographed on a silica gel column (acetone as eluent) to afford **2** as an orange solid ($R_f$ = 0.72, yield 73%). $C_{17}H_{20}N_3O_2$: calcd. C 68.43, H 6.76, N 14.08, O 10.72; found C 68.25, H 6.84, N 13.91, O 10.54.

**General Procedure for the Synthesis of Complexes 1a, 1b, 2a, and 2b:** A solution of the radical ligand (2.0 mmol) in acetonitrile (10 mL) was added to a solution of the appropriate triflate salt (1.0 mmol) in acetonitrile (15 mL). The color of the solution changed to dark green (for the $Cu^{II}$ complexes) or pale yellow (for the $Zn^{II}$ complexes). The resulting solution was filtered and $Et_2O$ vapor was slowly diffused into the solution. The single crystals obtained were suitable for X-ray studies.

**[Cu(CF$_3$SO$_3$)$_2$2$_2$] (1a):** Dark green blocks. $C_{32}H_{32}CuF_6N_6O_{10}S_2$: calcd. C 42.60, H 3.57, N 9.31; found C 42.68, H 3.57, N 9.34.

**[Cu(CF$_3$SO$_3$)$_2$2$_2$]·2CH$_3$CN (2a):** Efflorescent dark-green needles. $C_{40}H_{46}CuF_6N_8O_{10}S_2$: calcd. C 46.17, H 4.46, N 10.77; found C 44.19, H 4.31, N 8.39.

**[Zn(CF$_3$SO$_3$)$_2$1$_2$] (1b):** Yellow blocks. $C_{32}H_{32}F_6N_6O_{10}S_2Zn$: calcd. C 42.51, H 3.57, N 9.30; found C 42.57, H 3.59, N 9.19.

**[Zn(CF$_3$SO$_3$)$_2$2$_2$]·2CH$_3$CN (2b):** Efflorescent yellow needles. $C_{40}H_{46}F_6N_8O_{10}S_2Zn$: calcd. C 46.09, H 4.45, N 10.75; found C 44.55, H 4.26, N 9.15.

**X-ray Crystallographic Studies:** The measurements were performed on a Rigaku/MSC Mercury CCD diffractometer (for **1a**) or a Rigaku RAXIS imaging plate area detector (for **1b**, **2a**, and **2b**) with graphite-monochromated Mo-$K_\alpha$ radiation. The data were collected at a temperature of 103 K (for **1a**) or 123 K (for **1b**, **2a**, and **2b**) to a maximum $2\theta$ value of 54.9° (for **1a** and **2a**) or 60.1° (for **1b** and **2b**). After correction of the raw data for Lorentz and polarization effects, the structure was solved by direct methods (SIR97[35]). The non-hydrogen atoms were refined anisotropically. Hydrogen atoms were included but not refined. For **2a**, hydrogen atoms were refined isotropically. However, for **1a**, **1b**, and **2b** hydrogen atoms were included but not refined. Crystallographic data for these complexes are listed in Table 2.

CCDC-267140 (for **1a**), -267141 (for **2a**), -267142 (for **1b**), and -267143 (for **2b**) contain the supplementary crystallographic data for this paper. These data can be obtained free of charge from The Cambridge Crystallographic Data Center via www.ccdc.cam.ac.uk/data_request/cif.

**Magnetic Susceptibility Measurements:** The magnetic susceptibility was measured on polycrystalline samples of **1a** and **1b** or powder samples of **2a** and **2b** in the 2–300 K temperature range under a field of 500 G with a SQUID magnetometer (Quantum Design MPMS-5S). The data were corrected for magnetization of the sample holder and the magnetic susceptibility was corrected for diamagnetism of the constituent atoms using the Pacault method.[36]

**Calculational Methods:** Density functional theory (DFT) calculations were carried out by using a hybrid method (B3LYP) that combines Becke's three-parameter non-local exchange functional[21] with the non-local correlation functional of Parr and co-workers.[37] All of the computations were performed with the Gaussian 98 package[38] using the LANL2DZ basis set where the pseudopotential proposed by Hay and Wadt[39] is applied to the Cu atom, and the Dunning/Huzinaga valence double-ζ basis set[40] to the H, C, O, and N atoms. We employed the geometrical parameters of the isolated complex molecules of **1a** and **1b** determined by the X-ray crystallography as the geometry for the quantum chemical calculations, without geometry optimizations. DFT doublet, triplet, and quadruplet energies were calculated in straightforward unrestricted fashion (UB3LYP). The open-shell singlet energy for **1b** was estimated by the sum method.[41] Generally speaking, the UB3LYP calculations for the open-shell singlet state give the so-called

Table 2. Crystallographic data for **1a**, **1b**, **2a**, and **2b**.

| | **1a** | **1b** | **2a** | **2b** |
|---|---|---|---|---|
| Empirical formula | $C_{32}H_{32}CuF_6N_6O_{10}S_2$ | $C_{32}H_{32}F_6N_6O_{10}S_2Zn$ | $C_{40}H_{46}CuF_6N_8O_{10}S_2$ | $C_{40}H_{46}F_6N_8O_{10}S_2Zn$ |
| Formula mass | 902.30 | 904.13 | 1040.51 | 1042.34 |
| Crystal system | triclinic | triclinic | triclinic | triclinic |
| Space group | $P\bar{1}$ | $P\bar{1}$ | $P\bar{1}$ | $P\bar{1}$ |
| $a$ [Å] | 7.5928(5) | 7.6792(4) | 13.1699(8) | 12.2718(9) |
| $b$ [Å] | 11.050(1) | 11.1243(9) | 15.9376(8) | 12.9988(2) |
| $c$ [Å] | 12.656(2) | 12.3578(6) | 12.3034(6) | 16.309(1) |
| $\alpha$ [°] | 62.580(2) | 114.878(1) | 97.677(3) | 95.983(6) |
| $\beta$ [°] | 79.239(1) | 99.148(2) | 115.045(1) | 98.322(4) |
| $\gamma$ [°] | 86.508(1) | 93.366(3) | 95.896(1) | 114.940(4) |
| $V$ [Å$^3$] | 925.6(2) | 936.2(1) | 2281.9(2) | 2294.2(2) |
| $Z$ | 1 | 1 | 2 | 2 |
| $T$ [K] | 103 | 123 | 123 | 123 |
| $D_{calcd.}$ [g cm$^{-3}$] | 1.619 | 1.604 | 1.514 | 1.509 |
| Goodness of fit | 1.21 | 1.04 | 0.19 | 1.09 |
| $R$ | 0.051 | 0.047 | 0.038 | 0.074 |
| $R_W$ | 0.075 | 0.104 | 0.042 | 0.096 |

  

broken-symmetry state.[42] In the weak bonding regime, the following relationship is deduced between the energies of the broken-symmetry state ($E_{BS}$) and those of the pure (open-shell) singlet ($E_S$) and triplet states ($E_T$) from which we can estimate the pure singlet energy for complex **1b** [see Equation (7)].

$$E_{BS} = (E_S + E_T)/2 \quad (7)$$

## Acknowledgments

This work was supported by CREST (Core Research for Evolutional Science and Technology) of the Japan Science and Technology Agency (JST) and by a Grant-in-Aid for Scientific Research from the Japan Society for Promotion of Science (JSPS). Calculations were partly carried out at the Supercomputer Laboratory of the Institute for Chemical Research of Kyoto University.

[1] O. Kahn, *Molecular Magnetism*, Wiley-VCH, Weinheim, **1993**.
[2] A. Caneschi, D. Gatteschi, R. Sessoli, *Acc. Chem. Res.* **1989**, *22*, 392.
[3] A. Caneschi, D. Gatteschi, P. Rey, *Prog. Inorg. Chem.* **1991**, *39*, 331.
[4] C. G. Pierpont, C. G. Lange, *Prog. Inorg. Chem.* **1994**, *41*, 331.
[5] D. J. R. Brook, V. Lynch, B. Conklin, M. A. Fox, *J. Am. Chem. Soc.* **1997**, *119*, 5155.
[6] B. D. Koivisto, R. G. Hicks, *Coord. Chem. Rev.* **2005**, *249*, 2612.
[7] M. Jenings, K. E. Preuss, J. Wu, *Chem. Commun.* **2006**, 341.
[8] A. Caneschi, D. Gatteschi, P. Rey, R. Sessoli, *J. Am. Chem. Soc.* **1987**, *109*, 2191.
[9] D. Luneau, P. Rey, J. Laugier, P. Fries, A. Caneschi, D. Gatteschi, R. Sessoli, *J. Am. Chem. Soc.* **1991**, *113*, 1245.
[10] K. Inoue, H. Iwamura, *J. Am. Chem. Soc.* **1994**, *116*, 3173.
[11] K. Inoue, T. Hayamizu, H. Iwamura, D. Hashizume, Y. Ohashi, *J. Am. Chem. Soc.* **1996**, *118*, 1803.
[12] G. Francese, F. M. Romero, A. Neels, H. Stoeckli-Evans, S. Decurtins, *Inorg. Chem.* **2000**, *39*, 2087.
[13] D. Luneau, F. M. Romero, R. Ziessel, *Inorg. Chem.* **1998**, *37*, 5078.
[14] Y. Pei, A. Lang, P. Bergerat, O. Kahn, M. Fettouhi, L. Ouahab, *Inorg. Chem.* **1996**, *35*, 193.
[15] K. Fegy, D. Luneau, T. Ohm, C. Paulsen, P. Rey, *Angew. Chem. Int. Ed.* **1998**, *37*, 1270.
[16] K. E. Vostrikova, E. Belorizky, J. Pécaut, P. Rey, *Eur. J. Inorg. Chem.* **1999**, 1181.
[17] R. D. Shannon, *Acta Crystallogr., Sect. A* **1976**, *32*, 751.
[18] F. A. Cotton, G. Wilkinson, *Advanced Inorganic Chemistry*, Wiley, New York, **1980**.
[19] A. Bondi, *J. Phys. Chem.* **1964**, *68*, 441.
[20] B. Bleaney, K. Bowers, *Proc. R. Soc. London*, *Ser. A* **1952**, *214*, 451.
[21] S. Fokin, V. Ovcharenko, G. Romanenko, V. Ikorskii, *Inorg. Chem.* **2004**, *43*, 969.
[22] A. Caneschi, D. Gatteschi, A. Grand, J. Laugier, L. Pardi, P. Rey, *Inorg. Chem.* **1988**, *27*, 1031, and references cited therein.
[23] Y. Y. Lin, R. S. Drago, *Inorg. Chem.* **1972**, *11*, 1334.
[24] L. C. Porter, R. J. Doedens, *Inorg. Chem.* **1985**, *24*, 1006.
[25] K. Ragavachari, *Theor. Chem. Acc.* **2000**, *103*, 361 and references cited therein.
[26] L. Noodleman, *J. Chem. Phys.* **1981**, *74*, 5737.
[27] M. Nishino, S. Yamanaka, Y. Yoshioka, K. Yamaguchi, *J. Phys. Chem. A* **1997**, *101*, 705.
[28] E. Ruiz, J. Cano, S. Alvarez, P. Alemany, *J. Comput. Chem.* **1999**, *20*, 1391.
[29] T. Onishi, D. Yamaki, K. Yamaguchi, Y. Takano, *J. Chem. Phys.* **2003**, *118*, 9747.
[30] E. Ressouche, J.-X. Boucherle, B. Gillon, P. Rey, J. Schweizer, *J. Am. Chem. Soc.* **1993**, *115*, 3610.
[31] R. N. Musin, P. V. Schastnev, S. A. Malinovskaya, *Inorg. Chem.* **1992**, *31*, 4118.
[32] J. F. W. Keana, S. B. Keana, D. Beetham, *J. Am. Chem. Soc.* **1967**, *89*, 3055.
[33] G. R. Newkome, H. C. R. Taylor, F. R. Fronczek, T. J. Delord, *J. Org. Chem.* **1984**, *49*, 2961.
[34] G. R. Newkome, G. E. Kiefer, Y. A. Frere, M. Onishi, V. K. Gupta, F. R. Fronczek, *Organometallics* **1986**, *5*, 348.
[35] A. Altomare, M. C. Burla, M. Camalli, G. L. Cascarano, C. Giacovazzo, A. Guagliardi, A. G. G. Moliterni, G. Polidori, R. Spagna, *J. Appl. Crystallogr.* **1999**, *32*, 115.
[36] R. R. Gupta, *Landolt-Börnstein, New Series II* (Eds.: K.-H. Hellwege, A. M. Hellwege), Springer Verlag, Berlin, **1986**, vol. 16 (Diamagnetic Susceptibility).
[37] C. Lee, W. Yang, R. G. Parr, *Phys. Rev. B* **1998**, *37*, 785.
[38] M. J. Frisch, G. W. Trucks, H. B. Schlegel, G. E. Scuseria M. A. Robb, J. R. Cheeseman, V. G. Zakrzewski, J. A. Montgomery Jr, R. E. Stratmann, C. J. Burant, S. Dapprich, J. M. Millam, A. M. Daniels, K. N. Kudin, M. C. Strain, O. Farkas, J. Tomasi, V. Barone, M. Cossi, R. Cammi, B. Mennuchi, C. Pomelli, C. Adamo, S. Clifford, J. Ochterski, A. G. Petersson, Y. P. Ayala, Q. Cui, K. Morokuma, K. D. Malick, D. A. Rabuck, K. Raghavachari, B. J. Foresman, J. Cioslowski, J. V. Ortiz, B. B. Stefanov, G. Liu, A. Liashenko, P. Piskorz, I. Komaromi, R. Gomperts, R. L. Martin, D. J. Fox, T. Keith, M. A. Al-Laham, C. Y. Peng, A. Nanayakkara, V. G. Zakrzewski, M. Challacombe, P. Y. Ayala, W. Chen, M. W. Wong, J. L. Andres, C. Gonzalez, M. Head-Gordon, E. S. Replogle, J. A. Pople, *Gaussian 98*, *Revision A.9*, Gaussian Inc., Pittsburgh, PA, **1998**.
[39] P. J. Hay, W. R. Wadt, *J. Chem. Phys.* **1985**, *82*, 299.
[40] T. H. Dunning Jr, P. J. Hay, *Modern Theoretical Chemistry* (Ed.: H. F. Schafer, III), Plenum, New York, **1976**, vol. 3, pp. 1–28.
[41] C. J. Cramer, B. A. Smith, *J. Phys. Chem.* **1996**, *100*, 9664.
[42] J. Cano, P. Alemany, S. Alvarez, M. Verdaguer, E. Ruiz, *Chem. Eur. J.* **1998**, *4*, 476.

Received: January 27, 2006
Published Online: July 24, 2006

  